Journal of Cerebral Blood Flow & Metabolism (2015) 35, 371–381

www.jcbfm.com

RAPID COMMUNICATION

Rapid transport within cerebral perivascular spaces underlies widespread tracer distribution in the brain after intranasal administration

Jeffrey J Lochhead[1], Daniel J Wolak[1,2], Michelle E Pizzo[1,2] and Robert G Thorne[1,2,3,4,5]

The intranasal administration route is increasingly being used as a noninvasive method to bypass the blood–brain barrier because evidence suggests small fractions of nasally applied macromolecules may reach the brain directly via olfactory and trigeminal nerve components present in the nasal mucosa. Upon reaching the olfactory bulb (olfactory pathway) or brainstem (trigeminal pathway), intranasally delivered macromolecules appear to rapidly distribute within the brains of rodents and primates. The mechanisms responsible for this distribution have yet to be fully characterized. Here, we have used *ex vivo* fluorescence imaging to show that bulk flow within the perivascular space (PVS) of cerebral blood vessels contributes to the rapid central distribution of fluorescently labeled 3 and 10 kDa dextran tracers after intranasal administration in anesthetized adult rats. Comparison of tracer plasma levels and fluorescent signal distribution associated with the PVS of surface arteries and internal cerebral vessels showed that the intranasal route results in unique central access to the PVS not observed after matched intravascular dosing in separate animals. Intranasal targeting to the PVS was tracer size dependent and could be regulated by modifying nasal epithelial permeability. These results suggest cerebral perivascular convection likely has a key role in intranasal drug delivery to the brain.

Journal of Cerebral Blood Flow & Metabolism (2015) **35,** 371–381; doi:10.1038/jcbfm.2014.215; published online 10 December 2014

Keywords: blood–brain barrier; integrative optical imaging; matrix metalloproteinase-9; pharmacokinetics; pial vessels

INTRODUCTION

Biotherapeutic delivery to the brain remains a challenge because of the presence of the blood-brain barrier (BBB) and multiple blood-cerebrospinal fluid (CSF) barriers.[1] Growing evidence suggests the intranasal route of administration may allow biotherapeutics to bypass these barriers in rodents,[2] nonhuman primates,[3] and human beings.[4] A large body of preclinical and clinical work has shown central nervous system (CNS) delivery and/or central effects with peptides, proteins, gene vectors, and even mesenchymal stem cells after intranasal application.[5,6] Over the past decade, intranasal studies have increasingly focused on preclinical treatments in disease models (e.g., epidermal growth factor applied intranasally to chronically hypoxic mice[7] or various peptides applied intranasally after focal cerebral ischemia in rodents[8,9]), as well as clinical treatments for disorders such as Alzheimer's disease (e.g., intranasal insulin[10]), but the mechanisms and pathways governing transport of these substances from the nasal epithelia to widespread CNS areas have yet to be fully elucidated.

Much of what we know about how intranasally applied substances directly target the CNS has come from quantitative studies utilizing [^{125}I]-labeled proteins (e.g., Thorne *et al*[2]), typically by comparing brain levels and autoradiographic distributions after intranasal dosing against those resulting from matched intravascular controls (e.g., intravenous or intraarterial application of matched doses designed to approximate the area under the blood or plasma concentration time curve measured after intranasal delivery). These studies have suggested brain delivery occurs along two principal cranial nerve entry routes, the olfactory and trigeminal nerve-associated pathways, after paracellular or transcellular transport across the olfactory or respiratory epithelia (reviewed in Lochhead and Thorne[5,6]). A variety of classical tight junction proteins are present at the surface of the nasal epithelia (e.g., the apical olfactory epithelium is immunoreactive for zonula occludens-1 and -2, claudins-1, -3, and -5, and occludin[11]). The paracellular path is therefore thought to be increasingly restrictive for macromolecules with increasing hydrodynamic size; however, frequent turnover of constituent cells (and associated reepithelialization from basal cell division into mature olfactory sensory neurons and sustentacular cells of the olfactory epithelium or ciliated and goblet cells of the respiratory epithelium) may

[1]Division of Pharmaceutical Sciences, University of Wisconsin-Madison School of Pharmacy, Madison, Wisconsin, USA; [2]Clinical Neuroengineering Training Program, University of Wisconsin-Madison, Madison, Wisconsin, USA; [3]Neuroscience Training Program, University of Wisconsin-Madison, Madison, Wisconsin, USA; [4]Cellular and Molecular Pathology Training Program, University of Wisconsin-Madison, Madison, Wisconsin, USA and [5]The Institute for Clinical and Translational Research, University of Wisconsin-Madison, Madison, Wisconsin, USA. Correspondence: Dr RG Thorne, Division of Pharmaceutical Sciences, University of Wisconsin-Madison School of Pharmacy, 5113 Rennebohm Hall, 777 Highland Avenue, Madison, WI 53705, USA.
E-mail: rthorne@wisc.edu
This work was generously supported by the Wisconsin Alzheimer's Disease Research Center (NIH P50-AG033514), the Michael J Fox Foundation for Parkinson's Research, the Clinical and Translational Science Award program administered through the NIH National Center for Advancing Translational Sciences (NIH UL1TR000427 and KL2TR00428), the Wisconsin Alumni Research Foundation Accelerator Program, the University of Wisconsin-Madison School of Pharmacy, the Graduate School at the University of Wisconsin-Madison and fellowships through the Pharmaceutical Research and Manufacturers of America Foundation (DJW), the National Science Foundation Graduate Research Fellowship Program (DGE-1256259—MEP), and NIH National Research Service Awards (NRSA T32 EB011434) associated with the University of Wisconsin Clinical Neuroengineering Training Program (NRSA T32 EBO11424—DJW and MEP).
Received 11 August 2014; revised 17 October 2014; accepted 4 November 2014; published online 10 December 2014

regulate this restrictiveness.[5] After transport across the olfactory or respiratory epithelia to the lamina propria, experimental evidence indicates intranasally applied proteins can then access olfactory- or trigeminal-associated perineural, perivascular or lymphatic compartments connecting to the olfactory bulb region via perforations in the cribriform plate or to the brainstem region via the anterior lacerated foramen (rat).[2,5]

Brain levels of macromolecules after intranasal application have been measured to be orders of magnitude greater than levels measured after matched intravascular control dosing, consistent with the idea that intranasal delivery to the brain occurs by a direct process that effectively bypasses the systemic circulation and the BBB.[2] In light of this, the rapid kinetics of brain delivery and distribution after intranasal application of [^{125}I]-labeled proteins such as insulin-like growth factor-I (7.6 kDa) in rats[2] or interferon-β (20 kDa) in cynomolgus monkeys[3] is striking: within 30 to 60 minutes, peak levels in the nervous tissue of both species have been measured within the olfactory bulbs and trigeminal nerves but significant concentrations have also been measured in more distant cortical areas (e.g., in the motor cortex of rats), subcortical regions (e.g., in basal ganglia components of monkeys), and even the spinal cord (e.g., at upper cervical levels in both rats and monkeys). Similarly, studies in human beings have also exhibited rapid central delivery kinetics, with significant concentrations of intranasally applied peptides and proteins as large as insulin (5.8 kDa) reaching peak levels within 30 minutes in lumbar CSF despite no change in serum levels.[4] A key unanswered question concerns how substances may achieve rapid, widespread distribution throughout the neural axis after application to the nasal cavity by a mechanism not involving disposition through the bloodstream. It has been speculated that the rapid nature of central delivery observed after intranasal administration necessitates extracellular bulk flow (convection) because the observed kinetics and transport distances are inconsistent with rates of intracellular (axonal) transport within olfactory/trigeminal nerves or diffusion from the nasal application site;[5] indeed, a convective process would also help explain how intranasally applied substances can be delivered to distant cortical, subcortical, white matter, and spinal cord regions within 60 minutes of nasal application across species with brains of markedly different size (e.g., mice,[7] rats,[2] monkeys,[3] and human beings[4]).

Convective transport, the movement of a fluid volume and all the particles contained within it at a certain velocity,[12] has been clearly shown in only a few CNS compartments:[13–15] (i) CSF circulation within the brain's ventricles and subarachnoid spaces, (ii) CSF and interstitial fluid flow along certain cranial (e.g., olfactory[16]) and spinal nerve roots to extracranial lymphatics, and (iii) CSF and interstitial fluid flow within the perivascular space (PVS) of cerebral blood vessels. A number of lower molecular weight substances (e.g., peptides and smaller proteins such as insulin[4] as well as lower MW dextrans[17,18]) have been measured in sampled CSF shortly after transport across the nasal epithelia after intranasal administration;[6] however, several studies have failed to detect larger proteins in the CSF after intranasal administration (e.g., 7.6 kDa insulin-like growth factor-I, 25 kDa transforming growth factor-β1, and 38 kDa vascular endothelial growth factor), despite obtaining evidence of widespread distribution in sampled brain tissues.[2,19,20] The detection of high [^{125}I]-insulin-like growth factor-I levels in microdissected, perfusion-fixed cerebral blood vessels (the circle of Willis, basilar artery, and their associated branches) within 30 minutes after intranasal application has led to speculation that bulk flow within cerebral PVS may be involved in the rapid, widespread distribution of certain macromolecules within the brain after intranasal administration.[2]

Several groups have shown convective transport of tracers along cerebral PVS after injection into the brain, cisternal CSF, or directly into the PVS[21–24] but clear evidence confirming transport within the PVS after intranasal administration has not yet been reported. Here, we have used *ex vivo* fluorescence imaging and confocal microscopy to examine the localization of Texas Red-labeled 3 and 10 kDa lysine-fixable dextrans on the surface of the brain, as well as in interior brain regions after intranasal administration and compared this with the distribution after carefully matched intraarterial dosing. Our findings implicate rapid convection within the PVS of cerebral vessels as an important mechanism underlying the resulting brain distribution after intranasal delivery of macromolecules.

MATERIALS AND METHODS

Reagents

Purchased reagents included: lysine-fixable Texas Red-labeled 3 kDa dextran (TR-Dex3; 0.3 moles TR/mole dextran), 10 kDa dextran (TR-Dex10; 1 mole TR/mole dextran), and ProLong Gold anti-fade media (Invitrogen, Carlsbad, CA, USA); mouse anti-rat endothelial cell antigen-1 (Abcam, Cambridge, MA, USA); activated rat matrix metalloproteinase-9 (MMP-9; Sino Biological, Beijing, China); Formical-4 (Decal Chemical, Tallman, NY, USA); all other reagents and supplies were from Thermo Fisher Scientific (Waltham, MA, USA) or Sigma Aldrich (St Louis, MO, USA), unless noted.

Free Diffusion Measurements and Tracer Sizing Using Integrative Optical Imaging

We used the integrative optical imaging (IOI) method to measure the free diffusion of each tracer after pressure ejection into dilute (0.3%) NuSieve GTG agarose (FMC, Philadelphia, PA, USA), as described previously.[25–27] Briefly, this method used epifluorescence microscopy with a system consisting of an Olympus BX61WI microscope equipped with a water-immersion objective (UM PlanFl 10x, NA 0.3; Olympus, Center Valley, PA, USA), Texas Red filter set (Chroma, Bellows Falls, VT, USA), and a CCD camera (Cool-Snap HQ^2; Photometrics, Tucson, AZ, USA). Each tracer's diffusion was imaged over time after ejection from 3 to 6 μm diameter glass micropipettes (catalog 617000, A-M Systems, Carlsborg, WA, USA) using a 100- to 200-milli-second nitrogen pulse (Toohey Spritzer, Toohey, Fairfield, NJ, USA), approximating a point source (Figure 1A). Fluorescence intensity was then extracted from the diffusion images along each of six different axes and the upper 90% of the resulting curves were fitted to the diffusion equation (equation 2 in Thorne *et al*[26]) using a nonlinear simplex algorithm (Figure 1B). Fits yielded estimates for a parameter, γ_i, over a succession of times, t_i; linear regression of $\gamma_i^2/4$ upon t_i yielded a slope equal to the free diffusion coefficient (D). Highest and lowest D from the six axes were discarded to yield an average D value for each individual measurement from the remaining four axes.

Intranasal and Intraarterial Administration

All experimental protocols were approved by the Institutional Animal Care and Use Committee at the University of Wisconsin-Madison and performed in accordance with the National Institutes of Health *Guide for the Care and Use of Laboratory Animals* (8th edition; 2011). Female Sprague–Dawley rats (180 to 230 g; Harlan Sprague–Dawley, Indianapolis, IN, USA) were housed under a 12-hour light–dark cycle and fed *ad libitum*. Rats were anesthetized with an intraperitoneal injection of urethane (1.2 g/kg) and cannulated through the abdominal aorta for tracer administration, plasma sampling, and upper body perfusion. Body temperature was maintained at 37 °C with a homeothermic blanket (Harvard Apparatus, Holliston, MA, USA). Administration parameters are listed in Table 1. Rats were placed in the supine position and intranasally administered 48 μL TR-Dex3 to alternating nares in 12 μL drops every 5 minutes ($n = 24$). Intraarterial control rats were infused with 0.5 mL TR-Dex3 through the abdominal aorta over the course of 1 to 2 minutes ($n = 9$). TR-Dex10-treated rats were intranasally administered 24 μL saline ($n = 7$) or activated rat MMP-9 (100 nmol/L dissolved in saline; $n = 12$) to alternating nares in 6 μL drops every 5 minutes. Twenty minutes after intranasal administration was initiated, rats were intranasally administered 24 μL TR-Dex10 to alternating nares in 6 μL drops every 5 minutes. Intraarterial control rats were infused with 0.5 mL TR-Dex10 after intranasal administration of MMP-9 as described above ($n = 6$).

Quantification of Texas Red-Labeled Dextran Levels in Plasma Samples

Blood samples (0.4 mL or less) were drawn from the abdominal aorta every 10 minutes after intranasal or intraarterial administration of TR-Dex3 or TR-Dex10 and stored in a microcentrifuge tube with heparin on ice. Samples were then centrifuged at $3000 \times g$ for 10 minutes at 4 °C. Plasma was removed and TR-Dex3 or TR-Dex10 was quantified on a fluorescent plate reader (BMG Labtech, Cary, NC, USA) with excitation and emission filters set at 584 and 620 nm, respectively. Plasma samples collected before each experiment were quantified and used as a blank value and the concentration of TR-Dex3 or TR-Dex10 was calculated from a standard curve. The plasma area under the curve over the course of the experiment was calculated using the trapezoidal method.

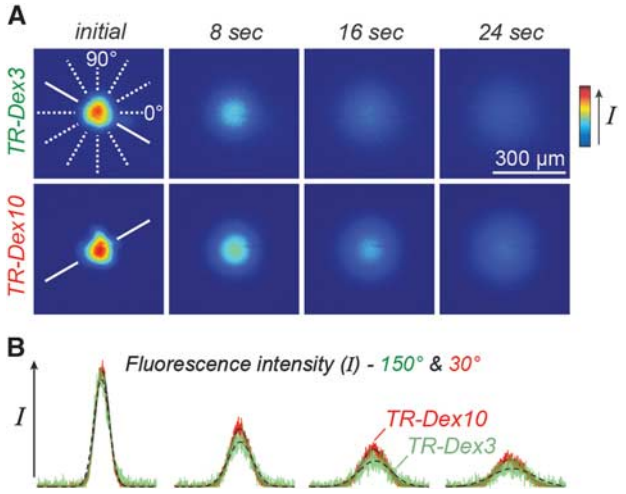

Figure 1. Characterization of tracer solution behavior by free diffusion measurements obtained using integrative optical imaging. (**A**) Representative images after pressure ejection of Texas Red-labeled 3 kDa dextran (TR-Dex3) or 10 kDa dextran (TR-Dex10) into dilute agarose. (**B**) Fluorescence intensity profiles were extracted from each image (TR-Dex3 data in green; TR-Dex10 data in red) and fit to the diffusion equation (dashed black lines, TR-Dex3 fits; solid black lines, TR-Dex10 fits) along one of six different axes (shown in **A**, solid white lines; 150° axis for TR-Dex3; 30° axis for TR-Dex10). Curve fitting yielded $D_{\text{TR-Dex3}}$ (37 °C) = 2.69×10^{-6} cm^2/second and $D_{\text{TR-Dex10}}$ (37 °C) = 1.35×10^{-6} cm^2/second for the records shown.

Ex Vivo Fluorescence Imaging of Cerebral Blood Vessels on the Brain Surface

Twenty minutes after initiation of intranasal or intraarterial administration of TR-Dex3 or 30 minutes after initiation of intranasal or intraarterial administration of TR-Dex10, rats were exsanguinated by perfusion through the abdominal aorta with 50 mL of ice-cold phosphate-buffered saline (PBS) before brain removal. The ventral brain surface was immediately viewed under an Olympus MVX10 Macroview fluorescent microscope equipped with a Texas Red filter (Chroma). Images of both treated and control animals were acquired at the same magnification and exposure time under the same light intensity with an Orca-flash 2.8 CMOS camera (Hamamatsu, Bridgewater, NJ, USA). Treated and control group images were merged into a single window and optimized in Adobe Photoshop using contrast and curves adjustments (Adobe Systems, San Jose, CA, USA). Identical adjustments were performed on all treatment groups. Using these images, the fluorescence intensity of TR-Dex3 in a region of interest in the PVS where the middle cerebral artery (MCA) branches from the anterior cerebral artery (ACA) was quantified using ImageJ software (Wayne Rasband, Research Services Branch, National Institutes of Mental Health, Bethesda, MD, USA). Images were optimized in Adobe Photoshop (Adobe Systems) with identical adjustments performed on all groups.

Processing of Brain Slices and Olfactory Epithelium

After treatment, rats were perfused through the abdominal aorta with 50 mL ice-cold PBS followed by 300 mL 4% paraformaldehyde in 0.1 mol/L phosphate buffer at room temperature. The brain was rapidly removed and 1-mm-thick coronal or sagittal slices were immediately imaged and processed in Photoshop as described above. In some experiments, the brain was postfixed in 4% paraformaldehyde in 0.1 mol/L phosphate buffer for 72 hours and 50 μm coronal sections were then sliced on a vibratome (Leica VT1000S, Wetzlar, Germany) and used for immunofluorescence. The olfactory epithelium was dissected, postfixed, and decalcified in Formical-4 for 24 hours at room temperature. Epithelia were then cryo-protected in 20% sucrose in PBS at 4 °C for 48 hours followed by snap freezing in isopentane on dry ice. Coronal sections (10 μm) were cut on a cryostat (Leica CM1950), mounted on glass slides, and coverslipped in ProLong Gold for confocal microscopy.

Immunofluorescence and Confocal Microscopy

Free-floating 50 μm coronal brain sections were washed in PBS and blocked for 1 hour in 5% goat serum in PBS (blocking buffer). Sections were then incubated in blocking buffer with mouse anti-rat endothelial cell antigen-1 (1:1000) for 2 hours at room temperature. Sections were washed in PBS and incubated for 1 hour in blocking buffer with DyLight 488 goat anti-mouse immunoglobulin G (1:200). After a final wash in PBS, sections

Table 1. Quantitative parameters for Texas Red-labeled lysine-fixable dextran tracers

	TR-Dex3	*TR-Dex10*
Approximate molecular weight (Da)	3,000	10,000
Free diffusion coefficient, D ($\times 10^{-7}$ cm^2/second; 37 ± 0.5 °C)	24.6 ± 0.20 (12)	15.6 ± 0.15 (13)
Hydrodynamic diameter, d_H (nm)[a]	2.67 ± 0.02	4.21 ± 0.04
Endpoint plasma sampling time after administration start (minutes)	20	30
Intranasal dextran concentration (mg/mL)[b]	25	50
Intranasal dextran dosing	4 × 12 μL drops	4 × 6 μL drops
Endpoint [plasma]$_{\text{intranasal}}$ (ng/mL)	21.1 ± 1.8 (5)	11.5 ± 1.4 (5)[c] 13.1 ± 1.8 (6)[d]
$AUC_{\text{intranasal}}$ (nmol/L · minutes)	48.7 ± 13.1 (5)	16.1 ± 2.3 (5)[c] 17.9 ± 3.7 (6)[d]
Intraarterial dextran concentration (μg/mL)[b]	4	0.4
Intraarterial dextran dosing	500 μL bolus	500 μL bolus
Endpoint [plasma]$_{\text{intraarterial}}$ (ng/mL)	92.8 ± 13.7 (5)	7.5 ± 0.3 (3)[e]
$AUC_{\text{intraarterial}}$ (nmol/L · minutes)	934.6 ± 89.2 (5)	36.7 ± 0.9 (3)[e]

Values reported as mean ± s.e.m. (n independent measurements). *AUC*, area under the plasma concentration-time curve from the start of dextran administration until the endpoint sample collection; TR-Dex3, Texas Red-labeled 3 kDa dextran. [a]Apparent hydrodynamic diameter determined from Stokes–Einstein equation [$d_H = (kT)/(3\pi\eta D)$, where k is Boltzmann's constant, T is absolute temperature, and η is the viscosity of water (6.9152×10^{-4} Pa second at $T = 310$ K)].[26] [b]Dissolved in saline. [c]Intranasal saline (4 × 6 μL drops) followed by intranasal TR-Dex10. [d]Intranasal matrix metalloproteinase-9 (100 nmol/L; 4 × 6 μL drops) followed by intranasal TR-Dex10. [e]Intranasal matrix metalloproteinase-9 (100 nmol/L; 4 × 6 μL drops) followed by intraarterial TR-Dex10.

were mounted onto glass slides and coverslipped in ProLong Gold. Laser scanning confocal microscopy was performed on brain slices or olfactory epithelial slices using an Olympus FV1000 confocal microscope (Olympus).

Quantification of MMP-9 Levels in CSF by Enzyme-Linked Immunosorbent Assay

Anesthetized rats were initially fixed in a stereotaxic frame (Stoelting, Wood Dale, IL, USA). A catheter made of 33 GA PEEK tubing (Plastics One, Roanoke, VA, USA) was connected to an infusion/withdrawal pump (Quintessential Stereotaxic Injector, Stoelting), inserted through the intact dura a distance of 1 mm into the cisterna magna, and sealed in place with cyanoacrylate. Animals were then carefully removed from the stereotaxic frame and placed in a supine position for intranasal administration of either 100 nmol/L MMP-9 or saline, as described above. Twenty minutes after intranasal administration was initiated, CSF was withdrawn at a constant rate (10 μL/minutes) for an additional 15 to 20 minutes while the supine position of the animals was maintained. CSF samples were centrifuged at 12,000 $\times g$ for 5 minutes at 4 °C and the supernatant was collected and stored at − 20 °C. Total MMP-9 CSF levels (active, pro-, and complexed protein) were then quantified using a commercial solid phase enzyme-linked immunosorbent assay (Rat Total MMP-9 Quantikine ELISA Kit, R&D Systems, Minneapolis, MN, USA) according to the manufacturer's instructions.

Statistical Analysis

All data were graphed and analyzed using SigmaPlot software (version 11.0, Systat Software, San Jose, CA, USA). Data were analyzed for statistical significance between treatment groups using a *t*-test or an analysis of variance test and are presented as means ± standard error (s.e.m.). A value of $P < 0.05$ was accepted as statistically significant.

RESULTS

Hydrodynamic Sizes of Lysine-Fixable Texas Red-Labeled Dextran Tracers

We chose to evaluate the intranasal delivery and subsequent brain distribution pathways of lysine-fixable Texas Red-labeled dextrans (3 kDa, TR-Dex3; 10 kDa, TR-Dex10) because these hydrophilic macromolecules are very soluble in water, allowing use of high concentrations with a correspondingly higher signal-to-noise for fluorescence imaging, as well as the option to be fixed by paraformaldehyde perfusion, negating postmortem tracer diffusion in tissue slices. Although the solution properties of a number of different fluorescently labeled dextrans have been extensively characterized (e.g., monomeric nature, diffusion behavior, and hydrodynamic diameters),[25–27] no such information yet exists to our knowledge for dextrans covalently modified with lysine residues. We therefore characterized the free diffusion coefficients (D) of TR-Dex3 and TR-Dex10 using IOI, an established and highly validated method for measuring the diffusion of fluorescently labeled macromolecules.[12] D values determined by IOI (Table 1) allowed us to estimate apparent hydrodynamic diameters (d_H) of 2.7 nm for TR-Dex3 and 4.2 nm for TR-Dex10 using the Stokes–Einstein equation (Table 1), in general agreement with past estimates using other nonlysine-fixable dextrans.[25,27] The results confirmed the stable, monomeric behavior of TR-Dex3 and TR-Dex10 in solution and provided quantitative estimates of their hydrodynamic size important for interpreting their disposition after intranasal delivery.

Rationale and Design of *In Vivo* Tracer Experiments for Fluorescence Imaging

Previous intranasal tracer studies have used fluorescent dextrans and confocal microscopy to examine the nasal epithelial transport of fluorescein isothiocyanate-labeled 3 and 10 kDa dextrans *in vivo*, showing significant transfer of 3 kDa dextran across the epithelia[28,29] but negligible transfer of 10 kDa dextran in the absence of the nasal absorption enhancer sodium taurodihydrofusidate.[29] Although one of these studies imaged the subsequent local transport of 3 kDa dextran in the connective tissue surrounding olfactory nerve bundles, with signal reaching to the olfactory bulb within 2 minutes of intranasal application,[28] detailed fluorescence imaging of dextran disposition on the brain surface or in brain sections beyond the olfactory bulb after intranasal dextran administration has not been described. We used Texas Red as opposed to fluorescein-labeled dextrans for our studies to reduce background autofluorescence and constrained the moles of Texas Red administered with intranasal solutions of TR-Dex3 (2.5 mmol/L TR in 48 μL) and TR-Dex10 (5 mmol/L TR in 24 μL). For transepithelial transfer, we ultimately found it necessary to use a nasal absorption enhancer with the 10 kDa dextran (applied as a 24 μL pretreatment just before intranasal TR-Dex10), but not the 3 kDa dextran, as in a prior study.[29] Rather than using sodium taurodihydrofusidate, a compound that enhances paracellular transport across the nasal epithelia but is associated with significant nasal irritation and toxic morphologic changes in nasal epithelial cells,[29] we evaluated the ability of MMP-9 to act as a physiologic absorption enhancer and a tool to enhance the nasal permeation and brain entry of TR-Dex10. MMP-9 is naturally expressed in a proteolytically active form in the olfactory epithelium,[30] where it appears to have a role in the reepithelialization and migration of new olfactory sensory neurons derived from basal cell turnover. It has previously been shown that MMP-9 is able to transiently increase the permeability of the perineurial barrier to deliver analgesic drugs in part through alteration of claudin-1,[31] which is also a component of tight junctions in the olfactory epithelium.[11] Total intranasal solution volumes and dropwise administration were essentially performed as previously described.[2] Important experimental parameters used in our study, including the TR-Dex3 and TR-Dex10 dosing regimens, are shown in Table 1. Intravascular controls with TR-Dex3 and TR-Dex10 were also performed similar to previous studies utilizing [^{125}I]-labeled protein tracers,[2] with intraarterial dosing matched to approximate or exceed plasma exposure after intranasal administration of TR-Dex3 or TR-Dex10 at the concentrations used to study brain disposition (Table 1). Our intraarterial control experiments therefore allowed us to compare potential brain entry or endothelial signal arising from the bloodstream with brain entry arising from direct pathways within the nasal lamina propria.

Visualizing Rat Cerebral Arteries and Their Associated Perivascular Spaces

The rat cerebral artery pattern on the ventral brain surface is shown schematically in Figure 2A. The anterior circulation includes the azygos ACA, paired MCAs, and paired nasal-olfactory arteries[32] (also called olfactory arteries[33,34]), among others.[14,34] The olfactory bulb arterial supply was of particular interest and includes the nasal-olfactory arteries (with major fields primarily in the nasal passages), the olfactofrontal arteries (providing blood supply to the dorsal olfactory bulbs), and the ventral olfactory arteries (providing blood supply to the ventral olfactory bulbs), all of which principally branch from the ACA.[32] The posterior circulation, arising from the paired vertebral arteries, includes the basilar artery, paired anterior inferior cerebellar arteries, numerous pontine ventral artery branches, paired superior cerebellar arteries, and paired posterior cerebral arteries, among others.[14,34] The schematized arterial pattern in Figure 2A may be readily realized in an unperfused (untreated) rat brain imaged shortly after being euthanized (Figure 2B). The PVS associated with numerous leptomeningeal (surface) arteries may be observed at higher magnification as a relatively clear fluid-filled space encircling a vascular lumen that appears red because of the iron-containing hemoglobin in erythrocytes (Figure 2B1); this PVS contains adventitial connective tissue elements and is thought to be bounded externally by fibroblast-like lining cells reflected from the

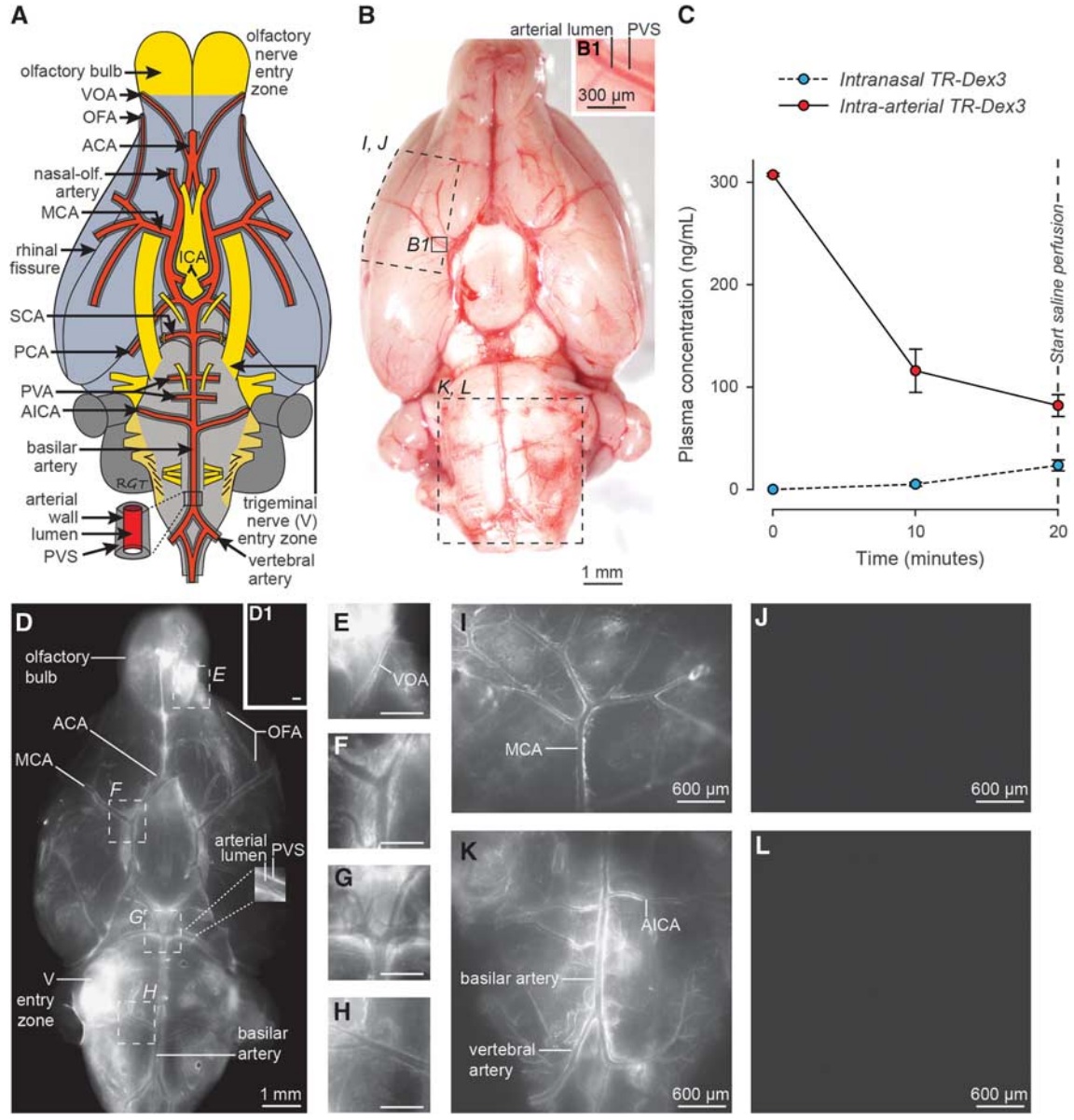

Figure 2. TR-Dex3 disposition in plasma and brain after intranasal or intraarterial administration. (**A**) Schematic of the ventral rat brain surface depicting key areas of focus for our study: the entry zones of cranial nerves I (olfactory) and V (trigeminal) along with the cerebral arteries and their associated PVS. (**B**) Ventral view of the unperfused brain surface from a nontreated animal showing the approximate regions imaged in (**I**–**L**). A putative PVS surrounding the lumen of numerous arteries can be realized upon close inspection because the vessels remain filled with blood. The PVS associated with a proximal branch of the MCA is indicated in B1. (**C**) TR-Dex3 plasma concentration over time after intranasal or intraarterial administration. Intranasal administration of 1.2 mg of TR-Dex3 was performed dropwise over 15 minutes. Intraarterial administration of 2 μg TR-Dex3 was infused through the abdominal aorta over the first 1 to 2 minutes of the experiment. Plasma samples were acquired at 10 and 20 minutes after initiation of the experiment. The concentration of TR-Dex3 at time zero after intraarterial administration was estimated by dividing the dose by the plasma volume of female Sprague–Dawley rats (3.4 mL/100 g).[40] Values are presented as means $\pm$ s.e.m. ($n = 5$ for each condition). (**D**) *Ex vivo* fluorescence imaging of the ventral brain surface after intranasal TR-Dex3 and saline upper body perfusion. Representative image showing TR-Dex3 fluorescent signal on the olfactory bulb, the trigeminal nerve (V) entry zone of the brainstem, and in the PVS of arteries on the ventral surface of the brain 20 minutes after intranasal administration. A representative image obtained under identical imaging and image processing conditions revealed no visible fluorescence on the ventral brain surface after intraarterial administration of TR-Dex3 (D1; scale bar = 1 mm). Boxes in **D** are shown at higher magnification (**E**–**H**), with significant perivascular fluorescent signal observed along the VOA at the ventrocaudal olfactory bulb (**E**), at the bifurcation of the ICA into the MCA and ACA (**F**), at the level of the basilar artery dividing into two trunks yielding the SCA and PCA within the interpeduncular fossa (**G**), and at the lateral branching of the AICA off of the basilar artery (**H**). Representative images of the lateral brain surface in different animals consistently revealed significant perivascular fluorescence associated with the MCA after intranasal (**I**) but not intraarterial (**J**) administration of TR-Dex3 under identical imaging and image processing conditions. Similarly, representative images of the ventral brainstem also consistently revealed significant perivascular fluorescence associated with the posterior circulation after intranasal (**K**) but not intraarterial (**L**) administration of TR-Dex3 under identical imaging and image processing conditions. Scale bars for **E**–**H** = 400 μm. ACA, anterior cerebral artery; AICA, anterior inferior cerebellar artery; ICA, internal carotid artery; MCA, middle cerebral artery; OFA, olfactofrontal artery; PCA, posterior cerebral artery; PVA, posterior ventral artery; PVS, perivascular space; SCA, superior cerebellar artery; TR-Dex3, Texas Red-labeled 3 kDa dextran; VOA, ventral olfactory artery.

brain's pia mater and internally by components of the tunica media (smooth muscle) associated with the artery's outer wall.[23]

Texas Red-Labeled 3 kDa Dextran Rapidly Distributes to Cerebral Perivascular Spaces After Intranasal but Not Intraarterial Administration

Figure 2C shows plasma levels of TR-Dex3 after intranasal or intraarterial administration over 20 minutes, after which animals were perfused and euthanized by exsanguination. Plasma levels in the intraarterial group were higher than the intranasal group at every time point measured. The area under the curve was significantly higher in the intraarterial group (934.6 ± 89.2 nmol/L · minutes) than in the intranasal group (48.7 ± 13.1 nmol/L · minutes) during the course of the experiment ($n = 5$; $P < 0.001$; Table 1).

We performed *ex vivo* fluorescence imaging to visualize the distribution of fluorescent signal associated with leptomeningeal vessels and the brain surface. Initial pilot experiments exhibited substantially more vessel-associated fluorescence when rats were vascularly perfused with only 50 mL PBS rather than with 50 mL PBS followed by 300 mL paraformaldehyde (likely because of TR-Dex3 wash-out from the PVS during the longer perfusion time); we therefore chose to perfuse rats only with PBS and rapidly image the brains within minutes of perfusion for surface imaging. Using identical conditions of animal perfusion, tissue processing, image acquisition, and image processing, we observed prominent brain surface or perivascular fluorescence in ~80% of animals after intranasal administration of TR-Dex3 (19 out of 24 rats examined), while no animals exhibited brain surface or perivascular fluorescence after intraarterial TR-Dex3 (0 out of 9 rats examined), despite significantly higher plasma exposure to TR-Dex3 in the intraarterial group. Figure 2D shows a representative image from an animal receiving intranasal TR-Dex3. Approximately 20 minutes after initial intranasal administration of TR-Dex3, we observed significant fluorescence on the ventral and lateral brain surfaces, including high levels at the entry points for the olfactory nerves (olfactory bulb) and the trigeminal nerves (pons), as well as in the PVS surrounding leptomeningeal vessels. The fluorescent signal associated with surface arteries (e.g., the posterior cerebral artery observed at higher magnification in the inset of Figure 2D) could essentially be seen as a reverse image of equivalent arteries imaged in the unperfused state in Figure 2B (e.g., the MCA observed at higher magnification in Figure 2B1): a bright signal emitting from the fluid-filled PVS encircling a relatively dark vascular lumen with minimal fluorescent signal. Perivascular fluorescence was particularly evident in olfactory vessel branches of the ACA (e.g., the olfactofrontal artery in Figure 2D and ventral olfactory artery in Figure 2E), numerous branches of the MCA (Figures 2D, 2F, and 2I), the basilar artery and its superior cerebellar artery and posterior cerebral artery branches (Figures 2D, 2G, and 2K), the anterior inferior cerebellar artery (Figures 2D, 2H, and 2K), and the vertebral arteries (Figures 2D and 2K). The rapid appearance of TR-dex3 in the PVS of cerebral arteries on the ventral and lateral brain surfaces suggests these arteries are involved in the widespread distribution of macromolecules in the brain after intranasal administration. We observed no obvious fluorescent signal on the surface of the brain after intraarterial administration (Figures 2D1, 2J, and 2L), suggesting the TR-Dex3 visualized on the brain surface and within the PVS of cerebral vessels observed after intranasal administration did not originate in the bloodstream and subsequently cross the BBB. Further, quantification of fluorescence intensity within the anterolateral PVS angle at the bifurcation of the internal carotid artery into the MCA and ACA (Figure 3A) was significantly higher (24.2-fold) after intranasal administration compared with intraarterial administration ($n = 4$; $P < 0.001$; Figure 3B).

After intranasal administration of TR-Dex3, widespread perivascular fluorescence of TR-Dex3 was observed in 1-mm-thick coronal brain sections after perfusion with PBS and subsequent perfusion with 4% paraformaldehyde to prevent postmortem tracer diffusion within the tissue slice (Figures 4A and 4C). A substantial amount of this fluorescence was lost after prolonged tissue storage in PBS or 4% paraformaldehyde > 24 hours (data not shown), possibly because the PVS contains less protein constituents available for cross-linking with dextran's lysine residues; this necessitated that sections be obtained and imaged immediately after perfusion. No fluorescence was observed in identically processed coronal slices after intraarterial administration of TR-Dex3 (Figures 4B and 4D). In sections through the primary somatosensory cortex (S1) of the parietal lobe (Figure 4A), the highest levels of TR-Dex3 seen after intranasal administration were observed on the pial brain surface in the vicinity of the subpial space. We also observed TR-Dex3 associated with putative cortical penetrating arteries, as well as interior microvessels and noticed markedly lower fluorescence in the less vascularized white matter (Figure 4A). These observations suggest TR-Dex3 accesses the PVS of arteries upstream of the cortical pial surface, spreads along the subpial space upon vessel penetration, and finally travels with the PVS of penetrating vessels deeper into the brain to the microvessel level. Diffuse periventricular fluorescence was also seen in the vicinity of the dorsal third ventricle and hippocampus after intranasal administration (Figure 4C), but not intraarterial administration (Figure 4D). Confocal microscopy of 50 μm thick sections through the S1 cortex (Figure 4E) or hippocampus (Figure 4F) immunolabeled for the rat endothelial plasma membrane marker rat endothelial cell antigen-1 showed intranasal TR-Dex3 signal was associated with the PVS of vessels with diameters corresponding to arterioles/venules (Figure 4E), as well as capillaries (Figure 4F). Although most fluorescent signal observed within the interior region of brain sections after intranasal TR-Dex3 appeared closely associated with the PVS of blood vessels, Figures 4A, 4C, 4E, and 4F also contained regions of diffuse TR-Dex3 in adjacent parenchyma and occasional gradients leading away from blood vessels, suggesting at least some portion of TR-Dex3 was able to migrate beyond the PVS.

Intranasally Applied Texas Red-Labeled 10 kDa Dextran Rapidly Distributes to Cerebral Perivascular Spaces Only with Absorption Enhancer Pretreatment

Figure 5A shows plasma levels of TR-Dex10 after intranasal or intraarterial administration over 30 minutes, after which animals

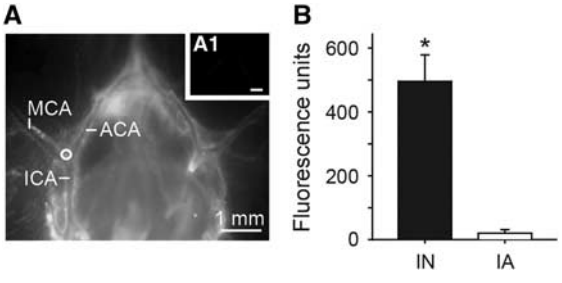

Figure 3. Perivascular fluorescent signal observed at the bifurcation of the internal carotid artery (ICA) into the middle cerebral artery (MCA) and anterior cerebral artery (ACA) was significantly greater after intranasal (IN) Texas Red-labeled 3 kDa dextran (TR-Dex3) (**A**) as compared with intraarterial (IA) TR-Dex3 (A1). Twenty minutes after IN or IA administration of TR-Dex3, rats were perfused with PBS and the brain was rapidly removed and images acquired under identical imaging and image processing conditions. Representative photomicrographs are shown with a circle indicating the region of interest used for quantification. (**B**) Fluorescence units quantified from the region of interest in rats after IN or IA administration ($n = 4$). Values are given as means ± s.e.m., *$P < 0.001$.

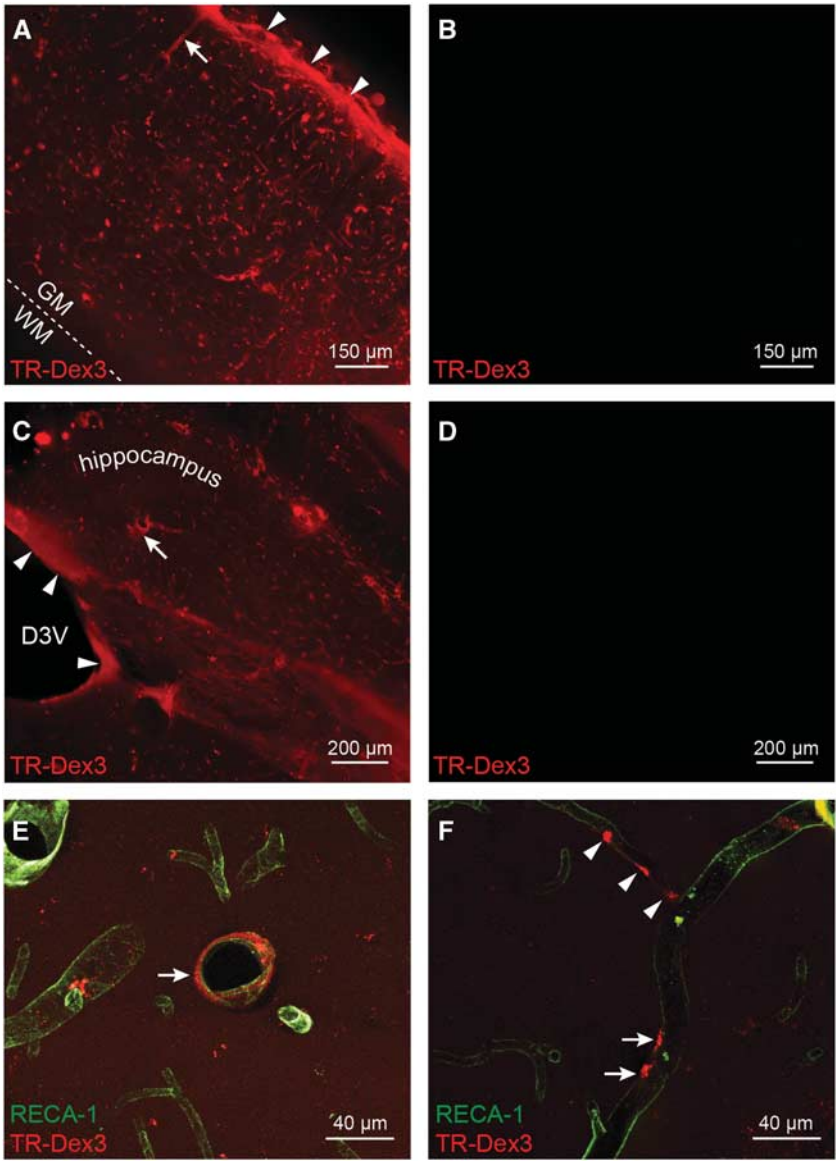

Figure 4. *Ex vivo* fluorescence imaging (**A**–**D**) and confocal imaging (**E** and **F**) of Texas Red-labeled 3 kDa dextran (TR-Dex3) fluorescence in brain sections 20 minutes after intranasal or intraarterial administration. (**A**) Intranasal TR-Dex3 resulted in significant fluorescent signal on the pial surface in the vicinity of the subpial space of the somatosensory (S1) cortex (arrow heads), as well as in perivascular spaces (PVSs) of vessels, including putative penetrating arteries (arrow). The dashed line represents the boundary between gray matter (GM) and the less vascularized white matter (WM). (**B**) Control rats administered TR-Dex3 intraarterially and imaged at the same level and settings as in **A** revealed no visible fluorescent signal. (**C**) TR-Dex3 can be found around the dorsal third ventricle (arrow heads), as well as in PVSs (arrow) in the hippocampus after intranasal administration. (**D**) Control rats administered TR-Dex3 intraarterially and imaged at the same level and settings as in **C** revealed no visible fluorescent signal. (**E**) Confocal imaging of a brain section from the S1/insular cortex reveals TR-Dex3 signal (red) surrounding a 35 μm diameter blood vessel after intranasal administration (arrow). Endothelial cells were identified by rat endothelial cell antigen-1 (RECA-1) immunofluorescence (green). (**F**) Confocal imaging of a brain section from the hippocampus revealed TR-Dex3 signal in the PVS of a 12 μm diameter blood vessel (arrows), as well as a putative capillary branch with a diameter of approximately 8 μm (arrow heads) after intranasal administration.

were perfused and euthanized by exsanguination. We chose to conduct our experiments with TR-Dex10 over 30 minutes instead of the 20-minute time point used for TR-Dex3 because TR-Dex10 plasma levels proved more reliably quantifiable at the 30-minute time point than at the 20-minute time point and this also allowed slightly additional time for nasal absorption enhancement with MMP-9. Intranasal pretreatment with saline or MMP-9 was initiated 20 minutes before rats were intranasally administered TR-Dex10. A separate group of rats were intraarterially administered TR-Dex10 after intranasal pretreatment of MMP-9 to control for the possibility that brain entry from the bloodstream may be affected in some way by intranasal MMP-9. The area under the curve after intraarterial administration (36.7 ± 1.6 nmol/L · minutes; $n = 3$) was significantly higher than the area under the curve after intranasal administration of TR-Dex10 with saline pretreatment (16.2 ± 8.3 nmol/L · minutes; $n = 5$) or MMP-9 pretreatment (17.9 ± 5.6 nmol/L · minutes; $n = 6$) ($P < 0.01$; Table 1).

Confocal imaging of tissue sections showed that intranasally administered TR-Dex10 signal was localized primarily at the surface of the olfactory epithelium after pretreatment with saline,

without visible signal anywhere within the lamina propria (Figure 5B). In contrast, intranasal pretreatment with MMP-9 allowed intranasally administered TR-Dex10 to be visualized well beyond the apical surface of the olfactory epithelium, with prominent signal observed in the lamina propria, within putative PVSs and nearby olfactory nerve bundles (Figure 5C). The results suggest TR-Dex10 did not easily cross the olfactory epithelial barrier without active nasal absorption enhancement, in agreement with previously published findings;[29] our results also support the use of MMP-9 as a fast-acting nasal absorption enhancer for TR-Dex10.

As with TR-Dex3, we performed *ex vivo* fluorescence imaging to visualize the distribution of fluorescent TR-Dex10 signal associated with leptomeningeal vessels on the brain surface, as well as in 1-mm-thick brain sections. Animals used for surface imaging were again perfused only with PBS, whereas animals used for tissue sections were perfused with both PBS and 4% paraformaldehyde to prevent postmortem tracer diffusion within the tissue slice. Using identical conditions of animal perfusion, tissue processing, image acquisition, and image processing, we observed prominent brain surface and perivascular fluorescence in over 80% of animals after intranasal administration of TR-Dex10 with MMP-9 pretreatment (10 out of 12 rats examined), compared with only 1 out of 7 rats intranasally administered TR-Dex10 with saline pretreatment and none of the 6 rats intraarterially administered TR-Dex10 after intranasal MMP-9 pretreatment. Further, the perivascular distribution of intranasally administered TR-Dex10 with MMP-9 pretreatment was qualitatively similar to the distribution observed with intranasal TR-Dex3 alone (described above). Perivascular fluorescence was prominently observed around leptomeningeal arteries on the ventral surface of the brain after intranasal administration of TR-Dex10 with MMP-9 pretreatment (Figures 5E and 5K). We also observed widespread perivascular fluorescence of TR-Dex10 in sagittal brain slices through the S1 cortex (Figure 5H) and brainstem (Figure 5N) after intranasal administration of TR-Dex10 with MMP-9 pretreatment. We rarely observed faint perivascular fluorescence on the surface of the brain (Figures 5D and 5J) and in sagittal brain slices at similar levels (Figures 5G and 5M) after intranasal administration of TR-Dex10 with saline pretreatment, suggesting TR-Dex10 encountered difficulty accessing direct pathways from the nasal lamina propria to the brain without active nasal absorption enhancement. No fluorescence was observed on the surface of the brain (Figures 5F and 5L) or in sagittal brain slices at similar levels (Figures 5I and 5O) after intraarterial administration of TR-Dex10 with intranasal pretreatment of MMP-9. This suggests the brain fluorescence we observed in rats pretreated with intranasal MMP-9 and intranasally administered TR-Dex10 was likely because of direct pathways from the nasal lamina propria to the brain, rather than through the bloodstream because of a possible MMP-9-mediated increase in BBB permeability. Intranasal pretreatment with MMP-9 was not expected to yield appreciable delivery of MMP-9 itself to the central compartment because the low applied MMP-9 concentration needed for local effects at the nasal epithelia (100 nmol/L) was orders of magnitude lower than the concentration of intranasally applied TR-Dex10 (5 mmol/L) used to show brain delivery. Separate experiments showed that CSF MMP-9 levels were unchanged with intranasal MMP-9 (CSF total MMP-9 measured by enzyme-linked immunosorbent assay, mean ± s.e.m.: intranasal saline, 30 ± 2 pg/mL, $n = 4$ animals; intranasal MMP-9, 34 ± 4 pg/mL, $n = 4$ animals; $P = 0.403$, *t*-test).

DISCUSSION

Our previous studies have shown that intranasally applied proteins achieve rapid, widespread distribution after brain entry along components associated with the olfactory and trigeminal nerves.[2,3] This study extends this prior work and provides several significant findings. First and most important, we provide the first direct evidence that convective transport within the cerebral PVS likely has an important role in rapid central distribution after intranasal administration. Specifically, our findings show that fluorescent signal associated with intranasal TR-Dex3 ($d_H = 2.7$ nm) prominently appears in the PVS of leptomeningeal arteries and interior vessels of both the anterior and posterior cerebral circulation within 20 minutes. We further show that fluorescent signal associated with intranasal TR-Dex10 ($d_H = 4.2$ nm) similarly appears in the PVS of the same vessels within 30 minutes, but only when administered after pretreatment with a nasal absorption enhancer such as MMP-9, implicating size-dependent transport of macromolecules across the nasal epithelia as a potential rate-limiting step to brain entry. Although along with others, we have previously detected macromolecules > 10 kDa in the brain after intranasal administration,[5,6] these experiments typically involved radiolabeled substances and methods with higher sensitivity than the fluorescence-based methods used here. Our discovery that MMP-9 pretreatment can enhance nasal epithelial permeation for TR-Dex10 was not entirely unexpected because MMP-9 has previously been shown to increase the permeability of the BBB, as well as the perineurial barrier of the sciatic nerve through modulation of tight junction (e.g., claudin-1) and basal lamina components (e.g., type IV collagen).[31,35] Finally, although we did not observe perivascular TR-Dex3 or TR-Dex10 fluorescence around surface vessels readily identifiable as veins based on morphologic considerations (e.g., vessel diameter and branching patterns), we cannot rule out their involvement in each tracer's central disposition.

It has been known for several decades that the PVS of cerebral blood vessels can potentially offer convective pathways for tracer distribution after central delivery.[13,21–23] Recent work by Iliff *et al*[24,36] has extended these findings in mice and rats using *in vivo* two-photon microscopy and *ex vivo* fluorescence imaging during and after intracisternal dextran tracer infusions; they show widespread CNS distribution of fluorescent dextran tracers within 30 minutes and suggest this distribution is in large part because of a convective flow within the PVS of surface and penetrating arteries driven by cerebral arterial pulsations in the direction of blood flow.[37] Our results appear consistent with this prior work but precisely how intranasally applied TR-Dex3, TR-Dex10 and other macromolecules may gain access to the PVS of cerebral blood vessels from the nasal mucosa is an open question. Several possibilities exist (Figure 6). Access to cerebral PVS pathways associated with the anterior and posterior circulations may occur through peripheral transport within perineural and/or lymphatic compartments that link up with the cerebral PVS. Dextrans have previously been detected in the CSF after intranasal administration[18] so it is possible that they may spill out of perineural or lymphatic compartments into the subarachnoid space CSF and, from there, gain access to PVSs as with intracisternal application.[24,36] Alternatively, peripheral entry into and transport within the PVS of olfactory and trigeminal nerve-associated blood vessels (e.g., the nasal-olfactory or trigeminal arteries) that connect directly with the cerebral PVS may be responsible for access to cerebral PVS pathways. PVS pathways associated with anastomotic vascular networks, for example, those located within the nasal passages[5] or those associated with the nasal-olfactory artery, olfactofrontal artery, or trigeminal artery,[6,14,32,34] may also have an important role in facilitating centrally directed PVS flow after intranasal application because PVS flow may occur in either direction in such networks.

It is well established that India ink, radiolabeled albumin, and other tracers can be found in the cerebral PVS, as well as the olfactory nerve, nasal lymphatic vessels, and the deep cervical lymph nodes after injection into the CSF or brain parenchyma.[22,38,39] These studies suggest a sequential transit of substances in the brain interstitial fluid or CSF along the PVS of

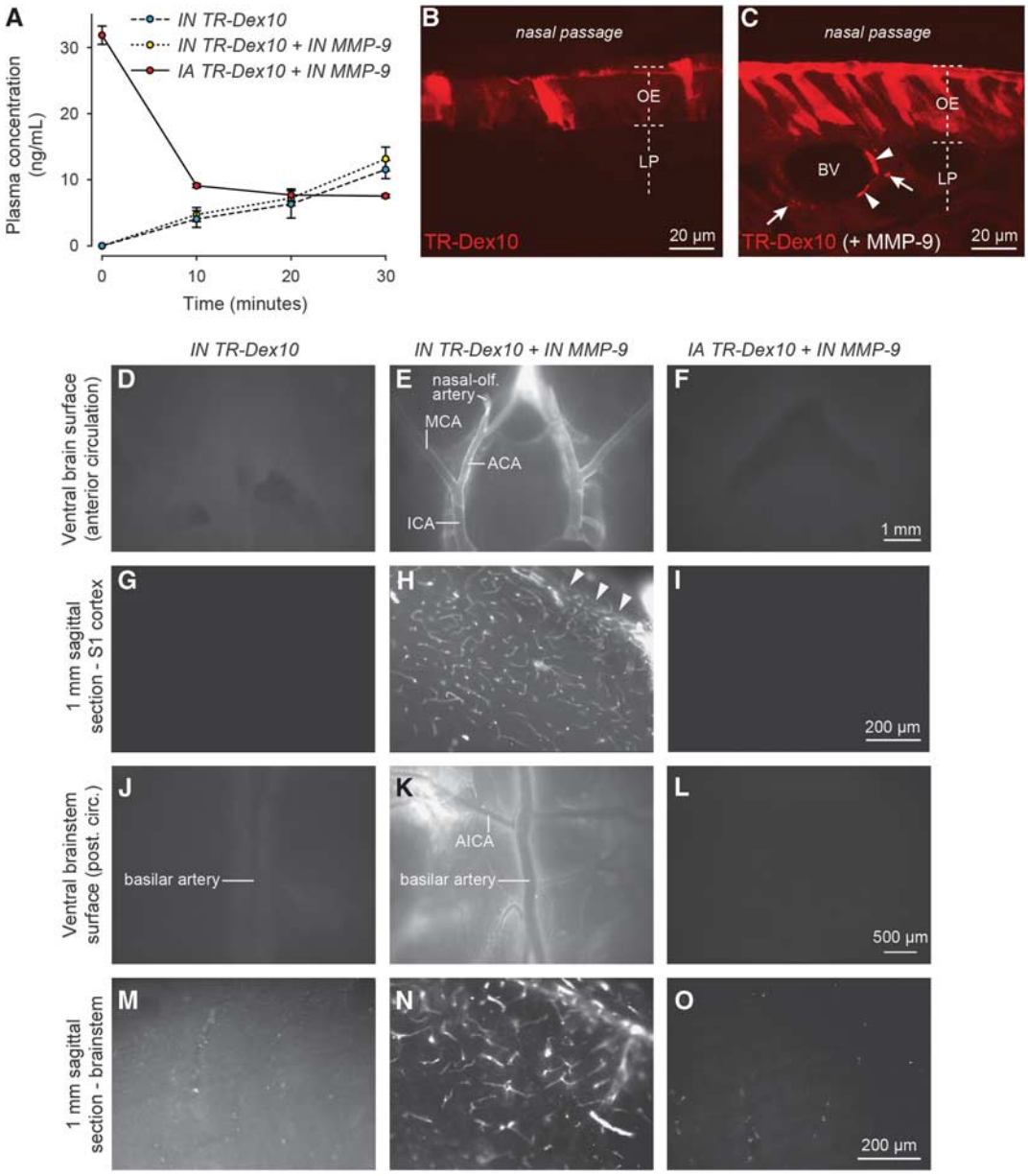

Figure 5. Texas Red-labeled 10 kDa dextran (TR-Dex10) disposition in plasma, olfactory epithelium, and brain after intranasal or intraarterial administration. (**A**) TR-Dex10 plasma concentration over time after intranasal (IN) or intraarterial (IA) administration. IN administration of 1.2 mg of TR-Dex10 was performed dropwise over 15 minutes after IN preadministration of saline or the nasal absorption enhancer matrix metalloproteinase-9 (MMP-9). Control animals were administered an IA bolus of 0.2 μg TR-Dex10 through the abdominal aorta over the first 1 to 2 minutes of the experiment after IN preadministration of MMP-9. Plasma samples were acquired at 10, 20, and 30 minutes after initiation of the experiment. The concentration of TR-Dex10 at time zero after IA administration was estimated by dividing the dose by the plasma volume of female Sprague–Dawley rats (3.4 mL/100 g).[40] Values are presented as means $\pm$ s.e.m. ($n = 3$ to 6 for each condition). (**B**) Confocal imaging (vertical cross section) of fluorescent signal in the olfactory epithelium (OE) and lamina propria (LP) 30 minutes after the initiation of IN TR-Dex10 with IN saline pretreatment. (**C**) Confocal imaging (vertical cross section) of fluorescent signal in the OE and LP 30 minutes after initiation of IN TR-Dex10 with IN MMP-9 pretreatment (imaging and image processing conditions identical to that in **B**). TR-Dex10 signal is markedly more apparent within the OE as well as in the LP with IN MMP-9 pretreatment; LP signal was prominent in the immediate vicinity of putative blood vessels (arrowheads) as well as in adjacent regions of the LP, likely in proximity to olfactory nerve bundles (arrows), as described previously for IN applied fluorescent 3 kDa dextran.[28] *Ex vivo* fluorescence imaging of the brains from animals receiving IN TR-Dex10 with IN saline pretreatment revealed only faint fluorescent signal on the brain surface (**D, J**) or in sagittal brain sections (**G, M**). In contrast, *ex vivo* fluorescence imaging of the brains from animals receiving IN TR-Dex10 with IN MMP-9 pretreatment revealed prominent, widespread perivascular fluorescent signal (**E**, **H**, **K, N**). Images of the ventral brain surface (**E**) and ventral brainstem (**K**) exhibited significant perivascular fluorescent signal along the internal carotid artery (ICA), middle cerebral artery (MCA), anterior cerebral artery (ACA), nasal-olfactory artery, and the anterior inferior cerebellar artery (AICA), among others. Images from sagittal brain sections through the primary somatosensory (S1) cortex (**H**) or brainstem (**N**) revealed significant fluorescent signal on the pial surface of S1 (arrowheads), as well as putative perivascular signal associated with numerous parenchymal blood vessels in both areas. *Ex vivo* fluorescence imaging of the brains from animals receiving IA TR-Dex10 with IN MMP-9 pretreatment revealed no visible fluorescent signal on the brain surface (**F, L**) or in sagittal brain sections (**I**), save for some sparse punctate signal in the brainstem (**O**). All images from specific regions were obtained under identical imaging and image processing conditions for the different treatment groups.

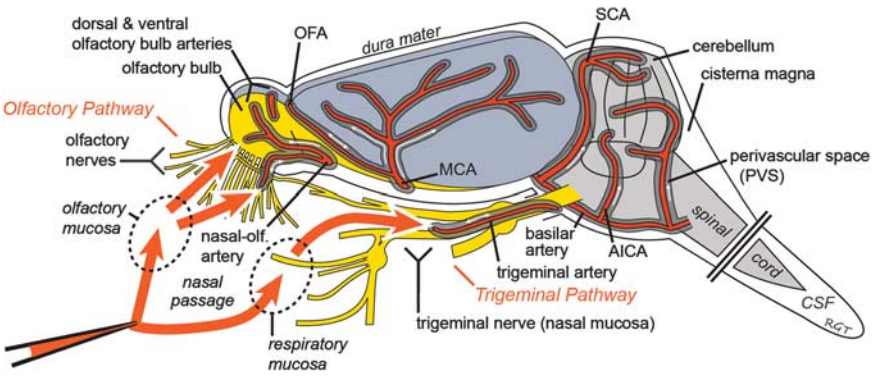

Figure 6. Proposed pathways involved in the extracellular transport of fluorescent dextran tracers and other substances from the nasal mucosa to widespread brain areas after intranasal administration. Prior work utilizing radiolabeled proteins in rats[2] and primates[3] has shown that small fractions of intranasally applied macromolecules may be transported via peripheral olfactory nerve-associated components (the olfactory pathway) to the olfactory bulbs and rostral brain regions or via peripheral trigeminal nerve-associated components (the trigeminal pathway) to the brainstem and caudal brain regions within 30 to 60 minutes of intranasal application. Intranasally applied substances capable of crossing the nasal epithelial barriers to the lamina propria of the olfactory or respiratory mucosa appear to access brain entry pathways associated with the olfactory and trigeminal nerves.[6] Use of experimental data along with simple mathematical modeling of the different possible transport mechanisms within these putative pathways has suggested that extracellular convection (bulk flow) within perineural, perivascular, or perilymphatic compartments is likely responsible for initial brain entry at the level of the olfactory bulbs and brainstem.[5] This study provides among the first direct evidence suggesting subsequent rapid widespread distribution of macromolecules throughout the brain from olfactory and trigeminal nerve-associated brain entry sites may at least partly be because of convection within the PVSs of cerebral vessels. See text for further explanation. AICA, anterior inferior cerebellar artery; CSF, cerebrospinal fluid; MCA, middle cerebral artery; OFA, olfactofrontal artery; PVS, perivascular space; SCA, superior cerebellar artery.

cerebral blood vessels, passage through the cribriform plate in compartments associated either with the PVS of vessels such as the nasal-olfactory artery or perineural spaces of olfactory nerves, and ultimate drainage into the deep cervical lymph nodes via nasal lymphatics. As discussed in detail elsewhere[2,3] and supported further by the present results, it appears increasingly likely that these previously shown transport pathways linking the cerebral PVS to lymphatics within the nasal lamina propria are potentially bidirectional and may depend on posture or other factors. One key issue concerns the directionality of bulk flow within the PVS of cerebral blood vessels, namely whether convection within the PVS occurs with or against the direction of blood flow. Previous attempts to model the direction of perivascular fluid flow have yielded conflicting results (reviewed in Lochhead and Thorne[5]). Ichimura *et al*[23] previously observed that tracer substances injected directly into the PVS of leptomeningeal arteries through an open cranial window 'moved back and forth, longitudinally, suggesting bulk flow of fluid within the PVS, which is slow and variable in direction.' Using *in vivo* two-photon microscopy with a closed cranial window preparation, Iliff *et al*[24] showed that fluorescent tracers initially appear to flow along arteries and arterioles penetrating into the brain after intracisternal injection, appearing at a later time within the PVS of veins. Further research is needed to resolve PVS transport biophysics in cerebral blood vessels. As already mentioned, anastomotic networks providing interarteriolar connections or direct links between arterioles and venules on the brain's surface may have a significant role in deciding the local direction of fluid flow within the PVS at any given moment; to the best of our knowledge, anastomotic networks have thus far received scant attention in this regard.

The cerebral PVSs are increasingly recognized as important extracellular pathways for the distribution of substances throughout the CNS. Our data suggest that in addition to acting as distribution pathways for centrally administered molecules, cerebral PVS are involved in the rapid transport of intranasally administered fluorescent tracers to widespread brain areas. We propose that intranasally administered substances, which are able to cross the nasal epithelial barrier and reach the lamina propria are then capable of reaching the brain along components associated with the olfactory and trigeminal nerves and, upon entry into the brain, rapidly distribute throughout the brain by convective PVS flow. The intranasal route of administration may therefore be a particularly attractive drug delivery method to treat diseases with cerebrovascular pathology, for example, Alzheimer's disease. The recent initiation of a large, multicenter phase II/III clinical trial testing intranasal insulin in mild cognitive impairment and Alzheimer's disease (clinicaltrials.gov), after an encouraging pilot trial by Craft *et al*,[10] further emphasizes the need to better understand how certain substances may target diverse sites within the CNS after their application intranasally. Our findings suggest future research focused on increasing the access of intranasally administered molecules to cerebral PVSs may yield improvements to the noninvasive targeting of biologic therapeutics to the CNS for clinical use.

DISCLOSURE/CONFLICT OF INTEREST

RGT acknowledges (i) periodically receiving honoraria for speaking to organizations within academia, foundations, and the biotechnology and pharmaceutical industry and (ii) occasional service as a consultant to industry on CNS drug delivery. JJL and RGT acknowledge being inventors on patents and/or patent applications related to intranasal drug delivery and/or the use of matrix metalloproteinases as intranasal absorption enhancers.

ACKNOWLEDGMENTS

The authors thank Chris Viesselmann, Katelyn Wees, and Justin Froze (University of Wisconsin-Madison) for technical assistance with histological processing and Niyanta Kumar (University of Wisconsin-Madison) for reviewing the manuscript.

REFERENCES

1 Neuwelt EA, Bauer B, Fahlke C, Fricker G, Iadecola C, Janigro D *et al.* Engaging neuroscience to advance translational research in brain barrier biology. *Nat Rev Neurosci* 2011; **12**: 169–182.
2 Thorne RG, Pronk GJ, Padmanabhan V, Frey WH, 2nd. Delivery of insulin-like growth factor-I to the rat brain and spinal cord along olfactory and trigeminal pathways following intranasal administration. *Neuroscience* 2004; **127**: 481–496.

3 Thorne RG, Hanson LR, Ross TM, Tung D, Frey WH, 2nd. Delivery of interferon-beta to the monkey nervous system following intranasal administration. *Neuroscience* 2008; **152**: 785–797.
4 Born J, Lange T, Kern W, McGregor GP, Bickel U, Fehm HL. Sniffing neuropeptides: a transnasal approach to the human brain. *Nat Neurosci* 2002; **5**: 514–516.
5 Lochhead JJ, Thorne RG. Intranasal delivery of biologics to the central nervous system. *Adv Drug Deliv Rev* 2012; **64**: 614–628.
6 Lochhead JJ, Thorne RG. Intranasal drug delivery to the brain. In: Hammarlund-Udenaes M, de Lange ECM, Thorne RG (eds). *Drug Delivery to the Brain*. Springer: New York, 2014. pp 401–431.
7 Scafidi J, Hammond TR, Scafidi S, Ritter J, Jablonska B, Roncal M *et al.* Intranasal epidermal growth factor treatment rescues neonatal brain injury. *Nature* 2014; **506**: 230–234.
8 Doyle KP, Yang T, Lessov NS, Ciesielski TM, Stevens SL, Simon RP *et al.* Nasal administration of osteopontin peptide mimetics confers neuroprotection in stroke. *J Cereb Blood Flow Metab* 2008; **28**: 1235–1248.
9 Luo Y, Shen H, Liu HS, Yu SJ, Reiner DJ, Harvey BK *et al.* CART peptide induces neuroregeneration in stroke rats. *J Cereb Blood Flow Metab* 2013; **33**: 300–310.
10 Craft S, Baker LD, Montine TJ, Minoshima S, Watson GS, Claxton A *et al.* Intranasal insulin therapy for Alzheimer disease and amnestic mild cognitive impairment: a pilot clinical trial. *Arch Neurol* 2012; **69**: 29–38.
11 Wolburg H, Wolburg-Buchholz K, Sam H, Horvat S, Deli MA, Mack AF. Epithelial and endothelial barriers in the olfactory region of the nasal cavity of the rat. *Histochem Cell Biol* 2008; **130**: 127–140.
12 Wolak DJ, Thorne RG. Diffusion of macromolecules in the brain: implications for drug delivery. *Mol Pharm* 2013; **10**: 1492–1504.
13 Abbott NJ. Evidence for bulk flow of brain interstitial fluid: significance for physiology and pathology. *Neurochem Int* 2004; **45**: 545–552.
14 Thorne RG. Primer on central nervous system structure/function and the vasculature, ventricular system, and fluids of the brain. In: Hammarlund-Udenaes M, De Lange ECM, Thorne RG (eds). *Drug Delivery to the Brain*. Springer: New York, 2014. pp 685–706.
15 Davson H, Segal MB (eds). *Physiology of the CSF and Blood-Brain Barriers*. CRC Press: Boca Raton, FL, 1996.
16 Bradbury MW, Cserr HF, Westrop RJ. Drainage of cerebral interstitial fluid into deep cervical lymph of the rabbit. *Am J Physiol* 1981; **240**: F329–F336.
17 in 't Veen JP, van den Berg MP, Romeijn SG, Verhoef JC, Merkus FW. Uptake of fluorescein isothiocyanate-labelled dextran into the CSF after intranasal and intravenous administration to rats. *Eur J Pharm Biopharm* 2005; **61**: 27–31.
18 Sakane T, Akizuki M, Taki Y, Yamashita S, Sezaki H, Nadai T. Direct drug transport from the rat nasal cavity to the cerebrospinal fluid: the relation to the molecular weight of drugs. *J Pharm Pharmacol* 1995; **47**: 379–381.
19 Yang JP, Liu HJ, Cheng SM, Wang ZL, Cheng X, Yu HX *et al.* Direct transport of VEGF from the nasal cavity to brain. *Neurosci Lett* 2009; **449**: 108–111.
20 Ma YP, Ma MM, Ge S, Guo RB, Zhang HJ, Frey WH, 2nd *et al.* Intranasally delivered TGF-beta1 enters brain and regulates gene expressions of its receptors in rats. *Brain Res Bull* 2007; **74**: 271–277.
21 Rennels ML, Gregory TF, Blaumanis OR, Fujimoto K, Grady PA. Evidence for a 'paravascular' fluid circulation in the mammalian central nervous system, provided by the rapid distribution of tracer protein throughout the brain from the subarachnoid space. *Brain Res* 1985; **326**: 47–63.
22 Zhang ET, Richards HK, Kida S, Weller RO. Directional and compartmentalised drainage of interstitial fluid and cerebrospinal fluid from the rat brain. *Acta Neuropathol* 1992; **83**: 233–239.
23 Ichimura T, Fraser PA, Cserr HF. Distribution of extracellular tracers in perivascular spaces of the rat brain. *Brain Res* 1991; **545**: 103–113.
24 Iliff JJ, Wang M, Liao Y, Plogg BA, Peng W, Gundersen GA *et al.* A paravascular pathway facilitates CSF flow through the brain parenchyma and the clearance of interstitial solutes, including amyloid beta. *Sci Transl Med* 2012; **4**: 147ra111.
25 Nicholson C, Tao L. Hindered diffusion of high molecular weight compounds in brain extracellular microenvironment measured with integrative optical imaging. *Biophys J* 1993; **65**: 2277–2290.
26 Thorne RG, Hrabetova S, Nicholson C. Diffusion of epidermal growth factor in rat brain extracellular space measured by integrative optical imaging. *J Neurophysiol* 2004; **92**: 3471–3481.
27 Thorne RG, Nicholson C. In vivo diffusion analysis with quantum dots and dextrans predicts the width of brain extracellular space. *Proc Natl Acad Sci USA* 2006; **103**: 5567–5572.
28 Jansson B, Bjork E. Visualization of in vivo olfactory uptake and transfer using fluorescein dextran. *J Drug Target* 2002; **10**: 379–386.
29 Marttin E, Verhoef JC, Cullander C, Romeijn SG, Nagelkerke JF, Merkus FW. Confocal laser scanning microscopic visualization of the transport of dextrans after nasal administration to rats: effects of absorption enhancers. *Pharm Res* 1997; **14**: 631–637.
30 Gueye Y, Ferhat L, Sbai O, Bianco J, Ould-Yahoui A, Bernard A *et al.* Trafficking and secretion of matrix metalloproteinase-2 in olfactory ensheathing glial cells: a role in cell migration? *Glia* 2011; **59**: 750–770.
31 Hackel D, Krug SM, Sauer RS, Mousa SA, Bocker A, Pflucke D *et al.* Transient opening of the perineurial barrier for analgesic drug delivery. *Proc Natl Acad Sci USA* 2012; **109**: E2018–E2027.
32 Coyle P. Arterial patterns of the rat rhinencephalon and related structures. *Exp Neurol* 1975; **49**: 671–690.
33 Brown JO. The morphology of circulus arteriosus cerebri in rats. *Anat Rec* 1966; **156**: 99–106.
34 Scremin OU. Cerebral Vascular System. In: Paxinos G (ed). *The Rat Nervous System*. 3rd edn. Elsevier Academic: Boston, 2004. pp 1167–1202.
35 Candelario-Jalil E, Yang Y, Rosenberg GA. Diverse roles of matrix metalloproteinases and tissue inhibitors of metalloproteinases in neuroinflammation and cerebral ischemia. *Neuroscience* 2009; **158**: 983–994.
36 Iliff JJ, Lee H, Yu M, Feng T, Logan J, Nedergaard M *et al.* Brain-wide pathway for waste clearance captured by contrast-enhanced MRI. *J Clin Invest* 2013; **123**: 1299–1309.
37 Iliff JJ, Wang M, Zeppenfeld DM, Venkataraman A, Plog BA, Liao Y *et al.* Cerebral arterial pulsation drives paravascular CSF-interstitial fluid exchange in the murine brain. *J Neurosci* 2013; **33**: 18190–18199.
38 Yamada S, DePasquale M, Patlak CS, Cserr HF. Albumin outflow into deep cervical lymph from different regions of rabbit brain. *Am J Physiol* 1991; **261**: H1197–H1204.
39 Walter BA, Valera VA, Takahashi S, Ushiki T. The olfactory route for cerebrospinal fluid drainage into the peripheral lymphatic system. *Neuropathol Appl Neurobiol* 2006; **32**: 388–396.
40 Everett NB, Simmons B, Lasher EP. Distribution of blood (Fe 59) and plasma (I 131) volumes of rats determined by liquid nitrogen freezing. *Circ Res* 1956; **4**: 419–424.